A. Arruti, A. Agote, J. Anzola, I. Aizpuru and M. Mazuela, "Impact of Non-Uniform Flux Density on Core Losses: A Case Study on Standard Core Geometries," *2024 Energy Conversion Congress & Expo Europe (ECCE Europe)*, Darmstadt, Germany, 2024, pp. 1-7.

DOI: https://doi.org/10.1109/ECCEEurope62508.2024.10752032

Impact of Non-Uniform Flux Density on Core Losses: A Case Study on Standard Core Geometries

Asier Arruti
Electronics and Computing Department
Mondragon Unibertsitatea
Hernani, Spain
aarruti@mondragon.edu

Anartz Agote
Electronics and Computing Department
Mondragon Unibertsitatea
Hernani, Spain
anartz.agote@alumni.mondragon.edu

Jon Anzola
Electronics and Computing Department
Mondragon Unibertsitatea
Bilbao, Spain
janzola@mondragon.edu

Iosu Aizpuru
Electronics and Computing Department
Mondragon Unibertsitatea
Hernani, Spain
iaizpuru@mondragon.edu

Mikel Mazuela
Electronics and Computing Department
Mondragon Unibertsitatea
Hernani, Spain
mmazuela@mondragon.edu

Abstract- The non-uniform flux density distribution inside magnetic cores leads to increased overall losses when compared to the commonly used uniform flux density assumption. This effect is amplified if rectangular based core shapes are used, where flux crowding in the corner sections plays a major role in the losses. To evaluate the effect of this non-uniform flux density distribution, computationally heavy FEM simulations are needed, in most cases incompatible with the preliminary design process of core selection. To solve this issue, this work analyses the flux distribution in a wide range of standard commercial core geometries and sizes with the aid of FEM simulations. The increment of losses between uniform and non-uniform flux densities are shown, allowing to quickly evaluate the impact of the flux distribution in the magnetic core selection process. Since the core losses depend on material parameters, these are evaluated in a wide range of the Steinmetz parameter *β*, based on typical ranges of the *β* parameter extracted from the open-source MagNet database.

Index Terms- Core loss, Magnetic flux, Magnetic cores, Ferrites.

I. Introduction

The magnetic devices (transformers and inductors) are key components for the design of power converters. These play a major role in the overall efficiency, power density, weight, and cost of the design [1]-[4], and should be accordingly designed for each specific application.

With the adoption of WBG transistor technology, the switching frequencies and power densities of the converters are being pushed beyond their traditional limits to achieve better performances [5], [6]. In this regard, the design of the magnetic devices is getting more difficult; the potential decrease in core power losses due to increased frequency is in most cases overshadowed by the reduction in the core size and cooling capabilities, resulting in higher temperatures [7]. Thus, the capacity to predict the magnetic device losses and temperatures accurately becomes more important than ever.

Although major advancements are being done to improve the accuracy of the loss estimations in magnetic cores [8]-[10], there are still other sources of error that are yet to be fully explored. These sources include, but are not limited to, discrepancies between equal cores, and the effects of size and geometry of the magnetic core, resulting in non-homogeneous flux distributions and flux crowding in the core losses. All these negatively impact the capabilities to accurately estimate the core losses, limiting the designers' capabilities to maximize the performance of magnetic devices.

The discrepancies between equal cores are unavoidable consequence of the manufacturing process of the cores. These discrepancies are expected to differ between core sizes and materials, thus accurately predicting their impact is in most cases infeasible. It falls to the designer to select and chose adequate safety factors, typically based on previous experience, to ensure a functional solution.

On the other hand, the effects of the geometry of the magnetic core, which can result in a non-homogeneous flux distribution, should, in theory, be able to be evaluated in the preliminary design process of the magnetic device. Nowadays, these effects can be evaluated in the final stages of the design process with the aid of Finite Element Method (FEM) simulators; after finding a suitable design a FEM simulation can be carried out to evaluate how the flux density distributes in the core geometry.

Using the simulations results, more accurate core loss estimations can be made, taking into account the non-

This work was supported by the Department of Education of the Basque Government under the Non Doctoral Research Staff Training Program through grant PRE_2020_1_0267. *(Corresponding author. Asier Arruti)*

homogeneous flux density distribution due to high frequency dimensional effects and flux crowding in the corner sections. Still, these simulations, unlike the analytical calculations used in the design process, are computationally expensive and thus not adequate for the preliminary design steps and core selection.

To address this issue, recently a simplified approach that captures the non-uniformities of the flux distribution was proposed [11]. Although this model cannot consider high frequency dimensional resonance effects, it accounts for the effects of non-homogeneous flux density distribution due to flux crowding and unbalanced magnetic areas in the core.

The approach from [11] uses a reluctance network model as an alternative to FEM simulations, resulting in an accurate representation of the flux distribution along the core (< 3 % error compared to FEM), while being much faster than FEM simulators (about 2700 times faster). Also, in [11] the reluctance network can be repurposed into a thermal resistance network, allowing to easily couple the loss and thermal models (about 2000 times faster than FEM). Still, there are some minor caveats regarding the methodology proposed in [11]:

- Three reluctance network admittance matrices (x, y and z axes) must be built to evaluate the flux distribution. This is not a major concern if only one core geometry (such as the custom geometry from [11] or cores of similar shapes are studied. If many different geometries (E/E, E/I, U/U, U/I, and toroid cores) are to be considered, building the admittance matrices for each shape and size becomes a cumbersome task.

- For the evaluation of the losses, according to [11], based on the orthogonality between axes, "...superposition of the losses in each dimension can be applied". This only holds true for losses proportional to the square of the flux density ($P_{\text{loss}} \propto B^{\beta}$ and $P_{\text{loss}} \propto B_x^{\beta} + B_y^{\beta} + B_z^{\beta}$ are only true for $\beta = 2$), which is not always the case. Thus, when using [11] the losses should be evaluated based on the modulus of the flux density vector instead of the orthogonality principle.

In this work, an alternative method to address the issue on the increment in power losses due to core geometry and non-uniform flux distribution is presented with the aim to facilitate the initial core selection process of a magnetic device design workflow. Unlike [11], this work will focus solely on standard core sizes, while also considering the dependency of core losses in the Steinmetz parameters based on experimental data available from the MagNet database [12]-[14].

In section II, FEM simulations of standard core geometries are used to obtain accurate representations of the non-uniform flux density distribution in the cores. Section III discusses the influence of the flux distribution and Steinmetz parameters in the core losses, analyzing 10 materials from the open-source MagNet database. Lastly, in section IV the results for standard E/ELP, U and toroid cores are presented in compact graphs so to be used in the core selection process. Tabulated polynomial coefficients are added to easily evaluate any of the specified geometries.

II. Evaluation of Non-Uniform Flux Distribution

To estimate the non-uniform flux distribution in the magnetic core, in this work 2-D FEM simulations are used. To do so Finite Element Method Magnetics (FEMM) [15] is used. The geometries tested include all the E/ELP, U and toroid cores available from the TDK Electronics ferrite product catalog [16]. The other core geometries require 3-D FEM simulations, which are beyond the scope of this work. The standard dimensions reported in the datasheets are used (the effect of tolerances is not considered).

Due to the complexity of the fringing field in gapped cores and the vast number of combinations achievable, the gapped version of E/ELP cores are not analyzed in this work. For cores with compatible I plate (information available in the datasheet, all ELP and certain U cores), both core/core and core/plate configurations are evaluated. The core mesh size is controlled so that it is at maximum the smallest of the core height or width length divided by 50, ensuring a fine resolution of the flux density distribution.

The core materials from the database [17]-[26] used in this work have a wide range of relative permeabilities, ranging from 900 to 10000. To ensure the value of relative permeability does not impact the results, comparisons between simulations with relative permeabilities of 500 and 1000000 have been tested, with discrepancies lower than 0.01 %

For the resistivity of the cores, which range from 0.1 Ωm up to 2 Ωm, the simulations have been evaluated at 0.1 Ωm and assuming a very high resistivity of 1 MΩm. The simulations are evaluated twice, in frequencies of 1 kHz and 1 MHz. The discrepancies introduced by these factors (between high resistivity and low frequency, and low resistivity and high frequency cases, is lower than the discrepancies due to relative permeability (<0.001 %).

All reported results are those regarding a case of initial permeability of 1000, core resistivity of 0.1 Ωm and frequency of 100 kHz.

The windings are modeled using square cross sections in E/ELP and U cores, taking 80 % of the core window height and width. In U cores the inwards current winding section is set in the core window, while the outwards current winding sections are divided into both sides of the core, maintaining equal core to winding distances and total winding area. For toroid cores the inwards winding section is modeled using a circle of 80 % of the core window diameter, while the outwards winding section takes the form of a ring of equivalent area at an equal core to winding distance.

Example of 2-D geometries simulated and resulting flux distributions are shown in Fig. 1.

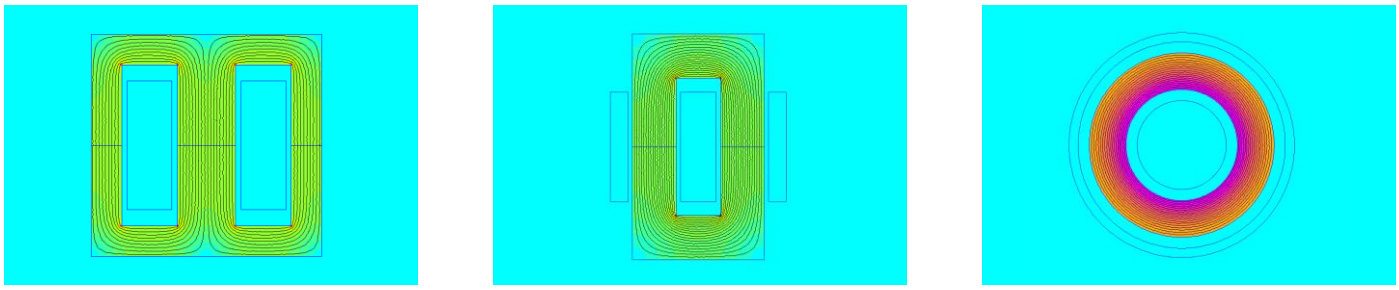

(a) (b) (c)

Fig. 1: Geometries and FEM simulation results for (a) E 88/38/20 in EE configuration, (b) U 30/26/26 in UU configuration, and (c) R 34.0 x 20.5 x 10.0 toroid.

III. Influence of Flux Distribution on Core Losses

As presented in the introduction, different models have been proposed to evaluate the core loss models under different conditions. An evaluation of all possible waveforms (sinusoidal, triangular, trapezoidal…) requires an extensive analysis beyond the focus of this paper, thus the basic form of the Steinmetz Equation (SE) [27] will be used. The choice of the SE over other versions is based on two points:

- The FEM simulator employed is based on sinusoidal excitation, thus the SE is intuitively the best fitted choice.
- Many of the other core loss modeling techniques, including the most common iGSE [28], are built upon the same basis of the SE, thus the conclusions achieved from the analysis with the SE should hold true for the other approaches.

In the SE, the losses (per unit of volume) are defined in the form of

$$P_{\text{loss}} = k \cdot f^{\alpha} \cdot B^{\beta}, \tag{1}$$

with f and B representing the frequency and flux density and α, β and k constituting the material and temperature specific Steinmetz parameters.

It can be deduced that the non-uniform flux density only affects the last multiplier term of (1), thus β is the only critical Steinmetz parameter for this analysis. Knowing that the core losses follow

$$P_{\text{loss,uniform}} \propto {B_{\text{uniform}}}^{\beta}, \tag{2}$$

$$P_{\text{loss,non-uniform}} \propto \frac{\sum_{i=1} V_i B_i^{\beta}}{V_{\text{core}}}, \tag{3}$$

for the uniform and non-uniform flux density cases, the relation between these is

$$\frac{P_{\text{loss,uniform}}}{P_{\text{loss,non-uniform}}} = \frac{V_{\text{core}} {B_{\text{uniform}}}^{\beta}}{\sum_{i=1} V_i B_i^{\beta}}. \tag{4}$$

Henceforth, this relation will be referred to as $F_{B,\text{dist}}$, simplifying the expression of non-uniform flux density power losses to

$$P_{\text{loss,non-uniform}} = F_{B,\text{dist}} \cdot P_{\text{loss,uniform}}. \tag{5}$$

For a given β value, $P_{\text{loss,non-uniform}}$ is directly evaluated from the FEM results, by first passing the flux density on the centroid of each element from FEMM to MATLAB and then solving (4). On the other hand, $P_{\text{loss,uniform}}$ requires the parameter B_{uniform} which is not defined yet. In this work, B_{uniform} has been defined so that the total magnetic energy in the core for both non-uniform and uniform cases is the same (equivalent inductance in both cases). Thus, the definition for B_{uniform} is then

$$B_{\text{uniform}} = \sqrt{\frac{\sum_{i=1} V_i B_i^2}{V_{\text{core}}}}. \tag{6}$$

Fig. 2 displays the resulting normalized flux density distribution for an EE80/38/20 core. The effect of flux crowding in the core corners is clear, with the magnetic equivalent uniform flux density being just slightly above a quarter of the peak flux density. Note that the flux density in the outside vertexes is also much lower than the uniform flux.

Due to both the power loss and magnetic energy equations being exponent functions (with powers of β and 2 respectively), the similarities between (3) and (4) result in $F_{B,\text{dist}} = 1$ for the case of $\beta = 2$. This denotes a critical point in core losses, where $\beta < 2$ leads to $F_{B,\text{dist}} < 1$ and $\beta > 2$ leads to

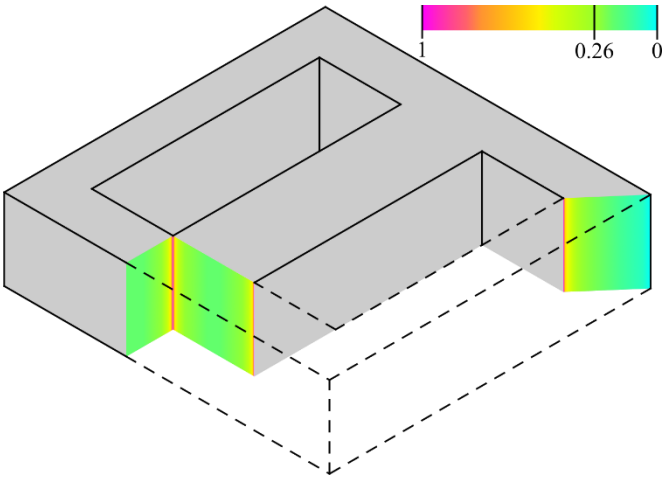

Fig. 2: Normalized non-uniform flux density distributions obtained from 2-D FEM simulations for an E/E structure, E80/38/20 core. The magnetic energy equivalent uniform flux density is 0.26 of the peak value.

$F_{B,\text{dist}} > 1$ (lower and higher losses than the uniform distribution assumption losses).

Lastly, the value of β must be defined to evaluate (4). It is well known that this parameter heavily depends on material, frequency, and working temperature [27], thus it makes more sense to analyze the impact of non-uniform flux density distribution as a function of β than focusing the analysis on a single value. To determine the range of interest for the parameter β, the sinusoidal data available from the MagNet database is used in this work [12]-[14].

To extract the values of β from the sinusoidal waveform core loss data, the same approach applied in [10] is used:

1. First, the available data is mapped to a 3-D space where xyz are $\ln(f)$, $\ln(B)$ and $\ln(P_{\text{loss}})$ respectively.
2. Then 3-D data distribution is fitted to a fifth-degree polynomial plane, thus $\exp\left(g_{(x,y)}\right) = P_{\text{loss}}$.
3. Afterwards, the derivative $g'_{(x,y)} = \partial g_{(x,y)}/\partial y$ is solved, which is straightforward for a polynomial function, resulting in an expression of β.
4. Lastly, $g'_{(x,y)}$ is evaluated for each datapoint available, resulting in a set of β values (one per datapoint) for each material and temperature.

All values of β obtained are represented by the shaded areas in Fig. 3 (classified by material and temperature). The darker a shaded area is the higher number of datapoints of β fall inside the denoted region. The β values extracted from the MagNet database range from 1.63 (3C90, 90 ºC) to 4.32 (3F4, 70 ºC). The average value of β is 2.55, with 98 % of the data falling in the range of $1.92 < \beta < 3.31$. Based on these results, the parameter $F_{B,\text{dist}}$ will be examined in the $\beta \in [1.5, 4.5]$ range.

Since the approach used is based on fifth-degree polynomials, these can lead to inaccuracies in edge cases. Thus, additionally two vertical lines are added to each shaded area, representing the boundaries for the 90$^{\text{th}}$ percentile. In these cases, the maximum and minimum values for β are 1.98 (3E6, 90 ºC) and 3.80 (3F4, 70 ºC) respectively. Thus, the $F_{B,\text{dist}}$ values outside of this range might lack practical meaning and should be taken carefully. Nonetheless, for the sake of completeness, results outside these boundaries are also reported.

IV. Obtained Results for Standard Cores

The evolution of $F_{B,\text{dist}}$ as a function of β is also represented in Fig. 3, where all cores tested are shown. Ideally, all cores would be labelled to facilitate data extraction from Fig. 3, but this is infeasible due to the number of cores tested. Thus, as an alternative, the data for each core is fitted to a third-degree polynomial equation. The fitting accuracy of these polynomial equations is in the range of –1.2 % to +0.6 %.

The results for the 41 toroid cores are detailed in TABLE I. Here, the $F_{B,\text{dist}}$ values at $\beta = 2.5$ and $\beta = 3.5$ are shown as well as the coefficient of the fitted polynomials. Using the averaged polynomial, errors of 1 %, 5 % and 10 % appear at β values 2.33, 3.17 and 3.86 respectively. Overall, considering that values of $\beta > 3.86$ are uncommon, excluding some outlier cases (Fig. 3, R 18.4 x 5.90 x 5.90 particularly), the influence of the non-uniform flux distribution has a mostly minor impact on toroid cores. This agrees with manufacturer using toroid cores in their core loss tests, whose low sizes also aid to minimize the potential impact of dimensional resonances.

TABLE I: Results for Toroid Cores

Core name	$F_{B,\text{dist}}$		$F_{B,\text{dist}} = p_0 + p_1\beta + p_2\beta^2 + p_3\beta^3$			
	β=2.5	β=3.5	p_0	p_1	p_2	p_3
R 2.50 x 1.50 x 1.00	1.0135	1.0577	0.0004	0.0085	-0.0173	0.9975
R 2.54 x 1.27 x 1.27	1.0249	1.1087	0.0014	0.0116	-0.0241	0.9906
R 3.05 x 1.27 x 1.27	**1.0398**	**1.1781**	**0.0038**	**0.0090**	**-0.0194**	**0.9728**
R 3.05 x 1.78 x 2.03	1.0150	1.0643	0.0005	0.0091	-0.0186	0.9969
R 3.43 x 1.78 x 1.78	1.0223	1.0969	0.0011	0.0113	-0.0233	0.9926
R 3.94 x 1.78 x 1.78	1.0327	1.1448	0.0025	0.0113	-0.0238	0.9826
R 3.94 x 2.24 x 1.30	1.0165	1.0710	0.0006	0.0097	-0.0198	0.9962
R 4.00 x 2.40 x 1.60	1.0135	1.0577	0.0004	0.0085	-0.0173	0.9975
R 5.84 x 3.05 x 1.52	1.0218	1.0949	0.0011	0.0112	-0.0231	0.9929
R 6.30 x 3.80 x 2.50	1.0132	1.0565	0.0004	0.0084	-0.0170	0.9976
R 8.00 x 4.00 x 4.00	1.0249	1.1087	0.0014	0.0116	-0.0241	0.9906
R 9.53 x 4.75 x 3.17	1.0251	1.1097	0.0014	0.0116	-0.0242	0.9904
R 10.0 x 6.00 x 4.00	1.0135	1.0577	0.0004	0.0085	-0.0173	0.9975
R 12.5 x 7.50 x 5.00	1.0135	1.0578	0.0004	0.0085	-0.0173	0.9975
R 12.7 x 7.90 x 6.35	1.0116	1.0497	0.0003	0.0076	-0.0154	0.9982
R 13.3 x 8.30 x 5.00	1.0114	1.0489	0.0003	0.0075	-0.0152	0.9982
R 14.0 x 9.00 x 5.00	1.0100	1.0428	0.0002	0.0068	-0.0137	0.9986
R 15.0 x 10.4 x 5.30	1.0069	1.0291	0.0001	0.0049	-0.0099	0.9994
R 15.8 x 8.90 x 4.70	1.0170	1.0734	0.0006	0.0099	-0.0202	0.9959
R 16.0 x 9.60 x 6.30	1.0135	1.0577	0.0004	0.0085	-0.0173	0.9975
R 17.0 x 10.7 x 6.80	1.0110	1.0471	0.0003	0.0073	-0.0148	0.9983
R 18.4 x 5.90 x 5.90	**1.0672**	**1.3140**	**0.0121**	**-0.0208**	**0.0411**	**0.9050**
R 20.0 x 10.0 x 10.00	1.0249	1.1087	0.0014	0.0116	-0.0241	0.9906
R 22.1 x 13.7 x 12.5	1.0118	1.0504	0.0003	0.0077	-0.0156	0.9981
R 22.6 x 14.7 x 9.20	1.0095	1.0405	0.0002	0.0065	-0.0131	0.9988
R 25.3 x 14.8 x 10.0	1.0148	1.0638	0.0005	0.0091	-0.0185	0.9969
R 29.5 x 19.0 x 14.9	1.0099	1.0424	0.0002	0.0067	-0.0136	0.9987
R 30.5 x 20.0 x 12.5	1.0091	1.0389	0.0002	0.0063	-0.0127	0.9989
R 34.0 x 20.5 x 10.0	1.0132	1.0566	0.0004	0.0084	-0.0170	0.9976
R 36.0 x 23.0 x 15.0	1.0103	1.0441	0.0002	0.0069	-0.0140	0.9985
R 38.1 x 19.05 x 12.7	1.0249	1.1087	0.0014	0.0116	-0.0241	0.9906
R 40.0 x 24.0 x 16.0	1.0135	1.0577	0.0004	0.0085	-0.0173	0.9975
R 41.8 x 26.2 x 12.5	1.0112	1.0480	0.0003	0.0074	-0.0150	0.9983
R 50.0 x 30.0 x 20.0	1.0135	1.0578	0.0004	0.0085	-0.0173	0.9975
R 58.3 x 32.0 x 18.0	1.0186	1.0804	0.0008	0.0104	-0.0213	0.9950
R 58.3 x 40.8 x 17.6	1.0065	1.0276	0.0001	0.0047	-0.0094	0.9994
R 63.0 x 38.0 x 25.0	1.0132	1.0565	0.0004	0.0084	-0.0170	0.9976
R 68.0 x 48.0 x 13.0	1.0062	1.0262	0.0001	0.0045	-0.0090	0.9995
R 87.0 x 54.3 x 13.5	1.0114	1.0489	0.0003	0.0075	-0.0153	0.9982
R 102 x 65.8 x 15.0	1.0099	1.0421	0.0002	0.0067	-0.0135	0.9987
R 140 x 103 x 25.0	1.0048	1.0202	0.0000	0.0035	-0.0071	0.9997
Average	1.0165	1.0719	0.0009	0.0077	-0.0158	0.9935

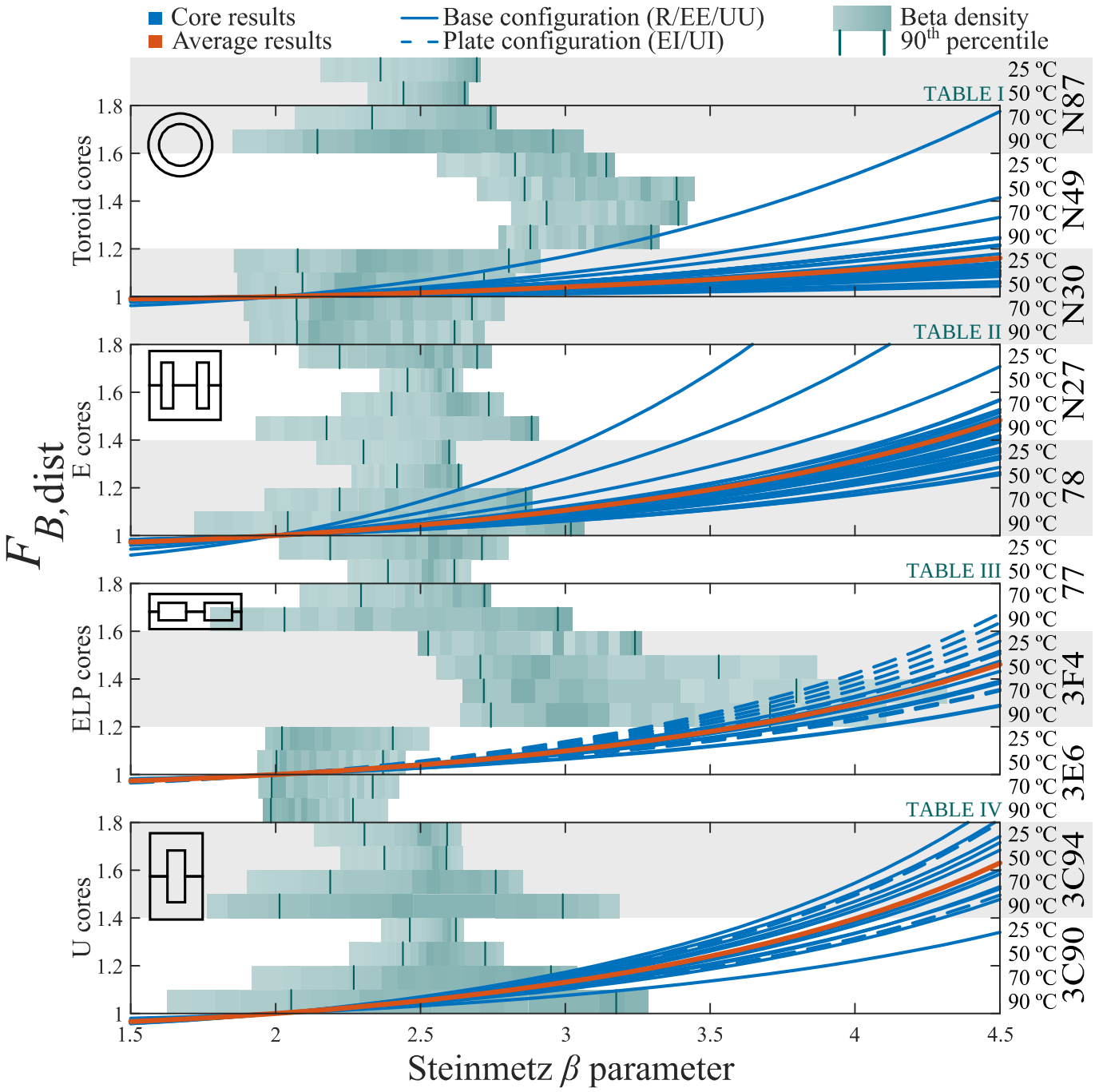

Fig. 3: β values extracted from the MagNet database and corresponding $F_{B,\mathrm{dist}}$ values for all toroid, E, ELP and U cores analyzed.

Additionally, a clear tendency between relation of inner and outer radius and influence of flux distribution exists, which makes sense considering that the closer the inner and outer radii are the more homogeneous the flux density is. The results for cores R 3.05 x 1.78 x 2.03, R 3.43 x 1.78 x 1.78 and R 3.94 x 1.78 x 1.78 from TABLE I clearly demonstrate this (for equivalent inner radius, the losses increase as the outer radius increases).

Although cataloged in the same section, the results for E/ELP cores are shown separately due to the noticeable geometrical differences between these. The 34 E cores are shown in TABLE II. Using the averaged polynomial, errors of 1 %, 5 % and 10 % appear at β values 2.11, 2.56 and 2.97 respectively. Due to the exponential nature of the loss increase and considering that values of $\beta > 2.97$ are not uncommon in certain materials (mainly N49 and 3F4), the non-uniform distribution can lead to noticeable underestimations of the core losses and should be considered in the core selection stages of the magnetic device design.

TABLE II: RESULTS FOR E CORES

Core name	$F_{B,\text{dist}}$		$F_{B,\text{dist}} = p_0 + p_1\beta + p_2\beta^2 + p_3\beta^3$			
	β=2.5	β=3.5	p_0	p_1	p_2	p_3
E 5	1.0309	1.1316	0.0066	-0.0257	0.0748	0.9013
E 6.3	**1.0955**	**1.4370**	**0.0248**	**-0.0947**	**0.2326**	**0.7181**
E 8.8	**1.1422**	**1.6805**	**0.0510**	**-0.2320**	**0.5386**	**0.4490**
E 10/5.5/5	1.0255	1.1070	0.0045	-0.0151	0.0486	0.9277
E 12.6/6.5/6.3	1.0371	1.1593	0.0086	-0.0356	0.1002	0.8743
E 12.7/6/6	1.0309	1.1336	0.0074	-0.0311	0.0860	0.8939
E 13/6.5/3.7	1.0361	1.1591	0.0100	-0.0443	0.1165	0.8659
E 13/6/6.15	1.0248	1.1068	0.0056	-0.0220	0.0623	0.9198
E 13/7/4	1.0371	1.1593	0.0086	-0.0356	0.1002	0.8743
E 14/8/4	1.0469	1.1966	0.0079	-0.0241	0.0801	0.8747
E 16/6/5	1.0448	1.2010	0.0143	-0.0676	0.1724	0.8136
E 16/7/5	1.0305	1.1315	0.0072	-0.0298	0.0832	0.8962
E 16/8/5	1.0366	1.1578	0.0088	-0.0366	0.1020	0.8739
E 19/8/5	1.0319	1.1387	0.0081	-0.0349	0.0947	0.8866
E 20/10/11	1.0374	1.1631	0.0098	-0.0425	0.1146	0.8643
E 20/9/6	1.0414	1.1808	0.0109	-0.0479	0.1287	0.8485
E 21/9/5	1.0335	1.1442	0.0078	-0.0321	0.0901	0.8870
E 22/15/6	1.0402	1.1625	0.0043	-0.0056	0.0383	0.9120
E 25/13/7	1.0392	1.1688	0.0092	-0.0381	0.1068	0.8666
E 25.4/10/7	1.0368	1.1607	0.0098	-0.0435	0.1165	0.8638
E 28/10/11	1.0454	1.2007	0.0131	-0.0594	0.1553	0.8246
E 30/15/7	1.0659	1.2887	0.0134	-0.0443	0.1234	0.8252
E 32/16/11	1.0387	1.1656	0.0087	-0.0354	0.1007	0.8716
E 34/14/9	1.0512	1.2178	0.0102	-0.0373	0.1109	0.8470
E 36/18/11	1.0428	1.1847	0.0100	-0.0406	0.1132	0.8577
E 42/21/15	1.0361	1.1566	0.0090	-0.0385	0.1055	0.8723
E 47/20/16	1.0478	1.2152	0.0157	-0.0753	0.1907	0.7965
E 40/16/12	1.0435	1.1933	0.0129	-0.0595	0.1543	0.8282
E 55/28/21	1.0418	1.1816	0.0106	-0.0460	0.1252	0.8501
E 56/24/19	1.0483	1.2171	0.0157	-0.0749	0.1902	0.7960
E 65/32/27	1.0402	1.1752	0.0106	-0.0464	0.1249	0.8529
E 70/33/32	1.0421	1.1854	0.0120	-0.0548	0.1439	0.8369
E 80/38/20	1.0312	1.1341	0.0072	-0.0292	0.0823	0.8959
E 100/60/28	1.0261	1.1138	0.0065	-0.0273	0.0738	0.9105
Average	1.0435	1.1915	0.0112	-0.0473	0.1259	0.8493

Due to more geometrical parameters (width of the yokes and outer and middle legs, core height to width relation), defining a direct relation between geometry and losses is more difficult than in the case of toroid cores. Still, when analyzing the outlier results (E 6.3 and E 8.8 cores), both have unbalanced outer and middle leg widths, resulting in a much higher flux density in the middle leg, which expectedly leads to increased losses. For design cases where losses are a major concern, for the typical windings structure presented in this paper, cores with unbalanced leg widths should be avoided (yoke widths included).

All 8 ELP cores analyzed have a compatible I plate, thus the results from TABLE III display both configurations separately. Using the averaged polynomial, errors of 1 %, 5 % and 10 % appear at β values 2.12, 2.59 and 3.02 respectively. From these results, the flux distribution can have a noticeable impact on the core losses and should be accordingly considered in the design process. Overall, the non-uniform flux distribution appears to have a similar impact in both E and ELP cores, with ELP cores being slightly more immune. When comparing ELP/ELP and ELP/I configurations, the average increment in losses for ELP/I configurations is around 25 % higher than for ELP/ELP structures.

Lastly, 11 U cores are examined, with two of these having compatible I plates as shown by TABLE IV. The averaged errors of 1 %, 5 % and 10 % appear at β values 2.08, 2.47 and 2.83 respectively. It can be concluded that the effect of the non-uniform flux distribution is worse than the previous geometries. For U/I configurations, the increment in the losses is about

TABLE III: RESULTS FOR ELP CORES

Core name	$F_{B,\text{dist}}$		$F_{B,\text{dist}} = p_0 + p_1\beta + p_2\beta^2 + p_3\beta^3$			
	β=2.5	β=3.5	p_0	p_1	p_2	p_3
ELP 18/4/10	1.0450	1.1998	0.0136	-0.0631	0.1634	0.8193
ELP 18/4/10 + plate	1.0563	1.2550	0.0192	-0.0932	0.2341	0.7543
ELP 22/6/16	1.0419	1.1851	0.0121	-0.0554	0.1451	0.8364
ELP 22/6/16 + plate	1.0537	1.2420	0.0176	-0.0842	0.2131	0.7727
ELP 32/6/20	1.0413	1.1819	0.0117	-0.0533	0.1401	0.8409
ELP 32/6/20 + plate	1.0508	1.2279	0.0162	-0.0767	0.1956	0.7890
ELP 38/8/25	1.0388	1.1704	0.0106	-0.0470	0.1247	0.8555
ELP 38/8/25 + plate	1.0479	1.2146	0.0150	-0.0708	0.1809	0.8035
ELP 43/10/28	1.0356	1.1555	0.0093	-0.0405	0.1089	0.8711
ELP 43/10/28 + plate	1.0440	1.1960	0.0132	-0.0611	0.1577	0.8254
ELP 58/11/38	1.0270	1.1165	0.0061	-0.0242	0.0680	0.9129
ELP 58/11/38 + plate	1.0318	1.1395	0.0082	-0.0352	0.0944	0.8876
ELP 64/10/50	1.0348	1.1518	0.0091	-0.0396	0.1068	0.8736
ELP 64/10/50 + plate	1.0415	1.1828	0.0114	-0.0509	0.1344	0.8452
ELP 102/20/38	1.0280	1.1195	0.0057	-0.0211	0.0623	0.9150
ELP 102/20/38 + plate	1.0339	1.1451	0.0075	-0.0296	0.0846	0.8905
Average	1.0408	1.1802	0.0116	-0.0524	0.1372	0.8442

TABLE IV: RESULTS FOR U CORES

Core name	$F_{B,\mathrm{dist}}$		$F_{B,\mathrm{dist}} = p_0 + p_1\beta + p_2\beta^2 + p_3\beta^3$			
	β=2.5	β=3.5	p_0	p_1	p_2	p_3
U 11/9/6	1.0480	1.2082	0.0121	-0.0524	0.1429	0.8285
U 15/11/6	1.0596	1.2697	0.0207	-0.1018	0.2561	0.7326
U 17/12/7	1.0636	1.2845	0.0200	-0.0942	0.2411	0.7378
U 20/16/7	1.0669	1.3041	0.0241	-0.1201	0.2999	0.6915
U 25/20/13	1.0582	1.2609	0.0189	-0.0912	0.2324	0.7512
U 26/22/16	1.0528	1.2335	0.0156	-0.0724	0.1887	0.7895
U 30/26/26	1.0500	1.2236	0.0160	-0.0767	0.1961	0.7887
U 93/76/16	1.0453	1.2029	0.0146	-0.0699	0.1782	0.8086
U 93/76/16 + plate	1.0640	1.2946	0.0250	-0.1281	0.3156	0.6850
U 101/76/30	1.0419	1.1852	0.0125	-0.0584	0.1519	0.8314
U 126/91/20	1.0314	1.1357	0.0079	-0.0340	0.0933	0.8877
U 126/91/20 + plate	1.0432	1.1917	0.0132	-0.0624	0.1618	0.8224
U 141/78/30	1.0697	1.3236	0.0286	-0.1481	0.3617	0.6445
Average	1.0534	1.2399	0.0176	-0.0851	0.2164	0.7696

50 % higher than the U/U structures, but since only 2 of 11 cores have compatible I plates, the sample size should be increased before defining a general trend.

V. CONCLUSIONS

In this work, the influence of the non-uniform flux density distribution in the magnetic cores is explored, focusing on standard toroid, E, ELP and U core geometries.

To do so, after ensuring that the influence of permeability, resistivity and frequency have negligible influence in the flux distribution (for the studied 10 materials), FEM simulations of each core geometry are carried out and the results are passed to MATLAB.

With the flux density module of each finite element available, the losses for each element are calculated individually and then the total core losses are added. This is repeated for the assumption of uniform flux density, and the differences between both cases are presented. Since the losses depend heavily on the Steinmetz parameters, the study present data for a $\beta \in [1.5, 4.5]$ range, which has been determined based in sinusoidal loss data for 10 materials and 4 temperatures from the MagNet open-source database.

All the results are presented in a compact graph, where the influence of core geometry, material and temperature can be easily visualized. To allow a more accurate estimation of the losses for a given standard core, the obtained curves are fitted to a third-degree polynomial and presented in tables.

Using the tabulated coefficients, the influence of geometrical effects like flux crowding on the core losses can be estimated, allowing a better comparison between cores of different geometries and sizes.

REFERENCES

[1] J. W. Kolar et al, "PWM Converter Power Density Barriers," *Power Conversion Conference* - Nagoya, Nagoya, Japan, 2007, pp. P-9-P-29,

[2] J. W. Kolar et al., "Exploring the pareto front of multi-objective single-phase PFC rectifier design optimization - 99.2% efficiency vs. 7kW/din3 power density," *IEEE 6th International Power Electronics and Motion Control Conference*, 2009.

[3] J. Mühlethaler et al, "Loss modeling of inductive components employed in power electronic systems," *8th International Conference on Power Electronics - ECCE Asia*, 2011.

[4] J. W. Kolar et al, "The ideal switch is not enough," *28th International Symposium on Power Semiconductor Devices and ICs (ISPSD)*, 2016

[5] M. Kasper et al, "GaN HEMTs Enabling Ultra-Compact and Highly Efficient 3kW 12V Server Power Supplies," *IEEE International Power Electronics and Application Conference and Exposition (PEAC)*, 2018.

[6] M. J. Kasper et al, "Ultra-high Power Density Server Supplies Employing GaN Power Semiconductors and PCB-Integrated Magnetics," *11th International Conference on Integrated Power Electronics Systems*, 2020.

[7] W. . -J. Gu et al, "A study of volume and weight vs. frequency for high-frequency transformers," *Proceedings of IEEE Power Electronics Specialist Conference*, 1993.

[8] J. Mühlethaler et al, "Improved core loss calculation for magnetic components employed in power electronic system," *2011 Twenty-Sixth Annual IEEE Applied Power Electronics Conference and Exposition (APEC)*, 2011.

[9] T. Guillod et al, "Calculation of Ferrite Core Losses with Arbitrary Waveforms using the Composite Waveform Hypothesis," *2023 IEEE Applied Power Electronics Conference and Exposition (APEC)*, 2023.

[10] A. Arruti et al, "The Composite Improved Generalized Steinmetz Equation (ciGSE): An Accurate Model Combining the Composite Waveform Hypothesis With Classical Approaches," in *IEEE Transactions on Power Electronics*, vol. 39.

[11] L. Clavero et al, "Improved Analytical Core Temperature Prediction Based on Estimation of the Non-Uniform Flux Distribution," *2023 25th European Conference on Power Electronics and Applications (EPE'23 ECCE Europe)*, 2023.

[12] D. Serrano et al., "Why MagNet: Quantifying the Complexity of Modeling Power Magnetic Material Characteristics," in *IEEE Transactions on Power Electronics*.

[13] H. Li et al., "How MagNet: Machine Learning Framework for Modeling Power Magnetic Material Characteristics," in *IEEE Transactions on Power Electronics*.

[14] H. Li et al, "MagNet-AI: Neural Network as Datasheet for Magnetics Modeling and Material Recommendation," in *IEEE Transactions on Power Electronics*.

[15] D. C. Meeker, Finite Element Method Magnetics, Version 4.2. AVAILABLE ONLINE.

[16] TDK Electronics ferrite product catalog, AVAILABLE ONLINE.

[17] TDK Electronics material N87 datasheet, AVAILABLE ONLINE.

[18] TDK Electronics material N49 datasheet, AVAILABLE ONLINE.

[19] TDK Electronics material N30 datasheet, AVAILABLE ONLINE.

[20] TDK Electronics material N27 datasheet, AVAILABLE ONLINE.

[21] Fair-Rite 77 material datasheet, AVAILABLE ONLINE.

[22] Fair-Rite 78 material datasheet, AVAILABLE ONLINE.

[23] Ferroxcube 3C94 material datasheet, AVAILABLE ONLINE.

[24] Ferroxcube 3C90 material datasheet, AVAILABLE ONLINE.

[25] Ferroxcube 3E6 material datasheet, AVAILABLE ONLINE.

[26] Ferroxcube 3F4 material datasheet, AVAILABLE ONLINE.

[27] S. A. Mulder, "Fit Formulae for Power Loss in Ferrites and their Use in Transformer Design," in proc. *26th International Power Conversion Conferenc*, 1993.

[28] K. Venkatachalam, C. R. Sullivan, T. Abdallah and H. Tacca, "Accurate prediction of ferrite core loss with nonsinusoidal waveforms using only Steinmetz parameters," *2002 IEEE Workshop on Computers in Power Electronics*, 2002.